Effective liquid drop description for the exotic decay of nuclei

M. Gonçalves* and S. B. Duarte
Conselho Nacional de Desenvolvimento Científico e Tecnológico-CNPq, Centro Brasileiro de Pesquisas Físicas (CBPF), Rua Dr. Xavier Sigaud 150, 22290-180 Rio de Janeiro, Brasil
(Received 23 February 1993)

The present model describes the exotic decay of nuclei considering the molecular phase of the fragments in an effective liquid drop description of the process. Shell corrections are included via experimental values of energy released in the disintegration (Q value), which is used to define the effective surface tension of the drop. The Coulomb potential energy is the exact solution of the Poisson equation for a uniform charge distribution in the nuclear volume. The inertial coefficient of the barrier penetrability problem is determined by using the Werner-Wheeler approximation for the velocity field of the nuclear flow. The model is successful in calculating the half-life for both the exotic decay and the α disintegration processes.

PACS number(s): 23.70.+j, 23.90.+Wg, 25.85.Ca

I. INTRODUCTION

Although the discovery of the nuclear fission dates from the 1930s, the high mass asymmetry in fission was found much later, during the 1970s. The first communications reporting the possible occurrence of a very asymmetric mass splitting of heavy nuclei appeared as results of the search for short-range nuclear tracks from ^{238}U in nuclear track emulsion [1–3]. These surprising results stimulated theoretical discussions, leading to the interpretation of the high mass asymmetry in fission as being generated by shell effects on the barrier penetrability due to the incidence of closed shells in the structure of one or both fragments [4,5]. The exploratory studies of this new radioactive decay mode were marked by the extensive calculations performed by Săndulescu, Poenaru, and Greiner [6], where several cluster emissions from heavy nuclei were predicted, and experimentally observed and confirmed later on. Experiments using solid-state counter telescopes by Rose and Jones [7] and Aleksandrov *et al.* [8] were successful in identifying the charge and mass of ^{14}C emitted from ^{223}Ra. These experiments, for the first time, established unambiguously the existence of exotic nuclear decay. Since then, many different models and theoretical estimates have appeared to explain the experimental results, and to predict new modes of such nuclear radioactive processes. Different nature and forms of the potential have been used in these models [9–12]. By adjusting the model parameters, results have led to a reasonable agreement with observations. The maximum deviations are within two orders of magnitude of experimental half-lives. The number of parameters in each model has been a consequence of the nature of the potential barrier used [10,11], or it depends on the adopted way in which the mass and charge vary in the precission phase [11,14]. In addition, it also depends on the semiempirical method of using the zero-point vibrational energy of the system [9,10].

In this work we calculate the half-life for exotic decays by considering a double spherical parametrization for the shape of the deformed nuclear system during the fission process. Although this shape parametrization has been used in other exotic decay models, for the first time we make use of an analytical closed expression to calculate the Coulomb energy of the molecular phase of the process [15]. The multidimensional evolution of the system is reduced to the one-dimensional case by geometrical constraints necessary to preserve the adopted shape during the whole process, and to keep the total volume of the system constant. In the reduced one-dimensional problem the Gamow penetrability factor [16] is calculated by using an effective mass, determined from the Werner-Wheeler approximation for the fluid velocity field of the nuclear flow. The present effective liquid scheme includes shell effects in the surface potential of the model, defining the surface tension of the drop in terms of the experimental energy released in the process (Q value). By using the minimal ingredients of a fissionlike description of the process, we get results in excellent agreement with experimental data for both exotic and α decay processes.

II. THE MODEL

A. Shape parametrization and potential

In the molecular phase of the process the geometrical configuration of the deformed system is approximated by two intersecting spheres with different radii. For the complete specification of this configuration it is necessary to have four independent coordinates, disregarding the location of the center of mass of the system. We show in Fig. 1 a sketch of a generic configuration where we specify our choice of coordinates: the radii of each spherical segment, R_1 and R_2, the height of the largest spherical segment, ξ, and the distance between their geometric centers, ζ. At the end of the prescission phase the system

*Present address: Departamento de Ciências Naturais, Fundação de Ensino Superior de São João del, Rei, Praça Dom Helvécio 74, 36300-000, São João del-Rei, MG, Brazil.

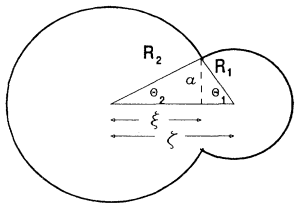

FIG. 1. Shape parametrization of nuclear deformation. The nascent cluster corresponds to the spherical segment with radius R_1, and the heavier daughter is represented by the spherical segment with radius R_2. The intersection of the spheres is a circumference with radius a, and ξ is the distance of the plane of the intersection to the geometrical center of the heavier fragment. The distance between the geometrical centers of the fragments is represented by ζ.

reaches a limiting configuration of two spherical tangent fragments with radii $\bar{R}_1$ and $\bar{R}_2$, respectively, for the cluster emitted and the heavier daughter.

To maintain the adopted shape parametrization for the deformed nuclear system, it is necessary to establish a geometric constraint,

$$R_1^2-(\zeta-\xi)^2=R_2^2-\xi^2 , \tag{1}$$

to keep the intersection of the spheres being the window for contact between fragments during the prescission phase. The constant total volume of the system is expressed in our coordinates by

$$2(R_1^3+R_2^3)+3[R_1^2(\zeta-\xi)+R_2^3\xi] -[(\zeta-\xi)^3+\xi^3]=4R_p^3 , \tag{2}$$

where R_p is the radius of the parent nucleus. During the development of the molecular phase of fragments we have taken a constant radius to the spherical segment corresponding to the nascent cluster; i.e., we have fixed $R_1=\bar{R}_1$.

The model considers explicitly the Coulomb and surface potential-energy contributions to the deformation energy of the system. Previous models for exotic decays have never used an analytical expression for the Coulomb energy during the prescission phase. In the most precise way the Coulomb energy has been taken into account by folding numerically nuclear charge densities in the volume of the fragments [9,17]. In our calculation we have made use of Gaudin's expression [15] for the electrostatic energy of spherical portions of uniform charge distribution,

$$V_C=\tfrac{8}{9}\pi a^5\varepsilon(x_1,x_2)\rho_c , \tag{3}$$

where ρ_c is the initial charge density and ε is a function of angular variables x_1 and x_2,

$$x_1=\pi-\theta_1 ,$$

$$x_2=\theta_2-\pi ,$$

which are defined in terms of the angles θ_1 and θ_2, shown in Fig. 1.

The expression for the ε factor in terms of auxiliary functions f and g is

$$\varepsilon(x_1,x_2)=\left[\frac{1}{\sin^2x_2}-\frac{1}{\sin^2x_1}\right]\left[\frac{f(x_2)}{\sin^2x_2}-\frac{f(x_1)}{\sin^2x_1}\right]-(\cot x_2+\cot x_1)\left[\frac{f'(x_2)+\pi/4}{\sin^2x_2}+\frac{f'(x_1)+\pi/4}{\sin^2x_1}\right] +\frac{1}{\sin^2x_1\sin^2x_2}\left[f(x_1+x_2)+\frac{1}{3}\sin^2(x_1+x_2)\right]+\frac{\pi}{8}[g(x_1)+g(x_2)] , \tag{4}$$

where f' denotes the derivative of f with respect to its argument. Explicitly, the auxiliary functions f, f', and g are given by

$$f(x)=1-x\cot x-\frac{\pi}{2}\tan\frac{x}{2} , \tag{5}$$

$$f'(x)+\frac{\pi}{4}=\frac{2x-\sin(2x)}{2\sin^2x}-\tan^2\frac{x}{2} , \tag{6}$$

$$g(x)=\left[1.5+\tan^2\frac{x}{2}+0.3\tan^4\frac{x}{2}\right]\tan\frac{x}{2}+\frac{2}{\sin^3x} , \tag{7}$$

where x assumes the values appearing as arguments of these auxiliary functions in (4). The above expression for the Coulomb energy is the exact solution of the Poisson equation for uniform charge distribution in the system volume [15].

For the surface potential we have introduced an effective surface tension σ_{eff} to the deformed system, defined through the equation

$$\frac{3}{5}e^2\left[\frac{Z_p^2}{R_p}-\frac{Z_1^2}{\bar{R}_1}-\frac{Z_2^2}{\bar{R}_2}\right]+4\pi\sigma_{\text{eff}}(R_p^2-\bar{R}_1^2-\bar{R}_2^2)=Q , \tag{8}$$

where Z_pe and Z_ie ($i=1,2$) are the nuclear charges, respectively, of the parent nucleus and the resulting fragments. This definition establishes that the difference between the energies of the initial and final configurations of the system reproduces the energy released in the disintegration, $Q=M-M_1-M_2$. The masses in the Q-value expression were taken from the 1983 atomic mass evaluation by Wapstra and Audi [18]. Therefore, for the surface potential we have

$$V_s=\sigma_{\text{eff}}(S_1+S_2) , \tag{9}$$

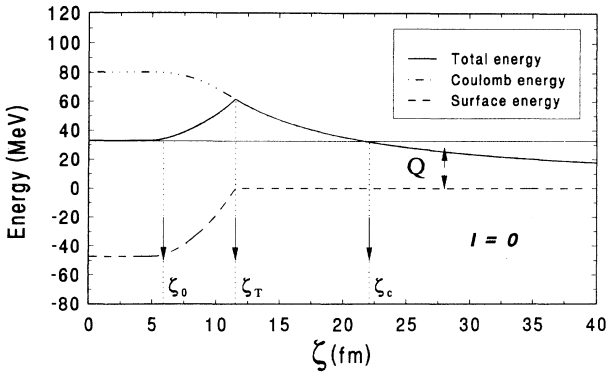

FIG. 2. One-dimensional potential barrier. The Coulomb energy is represented by the dot-dashed curve, and the surface by the dashed one. The total potential is the continuous curve.

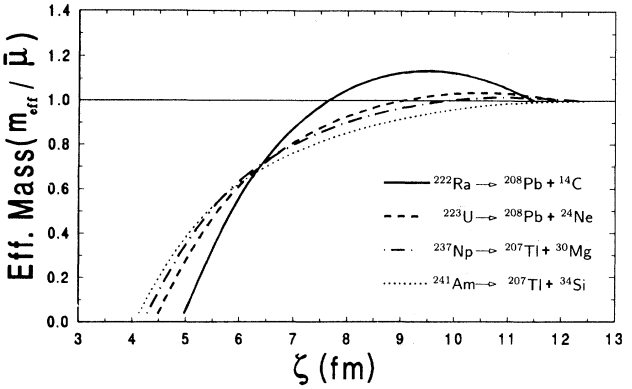

FIG. 3. The Werner-Wheeler effective mass for different cluster emissions as a function of the distance between the geometrical centers of the spherical segments. After the scission point the effective mass $\bar{\mu}$ is constant and equal to the reduced mass of separated fragments.

with the surface of each spherical segment given by

$$S_i=\pi R_i(R_i+\delta_i)\ , \tag{10}$$

where

$$\delta_i=\begin{cases}\zeta-\xi, & i=1\ ,\\ \xi, & i=2\ .\end{cases} \tag{11}$$

The effect of the centrifugal potential in the molecular phase cannot be discussed without a careful analysis of angular momentum transfer in the hydrodynamic flow of the nuclear fluid. In a simplifying assumption all models which take this contribution into account have considered it after the scission point only:

$$V_l=\frac{\hbar^2}{2\bar{\mu}}\frac{l(l+1)}{\zeta^2}\ . \tag{12}$$

In this approximation, the effect of the centrifugal potential on the half-life for exotic decays is completely negligible [19,20]. The reduced mass $\bar{\mu}=M_1M_2/(M_1+M_2)$ defines the rotational inertia of the system after scission point.

In Fig. 2 our one-dimensional potential is shown,

$$V=V_c+V_s+V_l-V_0\ , \tag{13}$$

provided with the constraints given by Eqs. (1) and (2) and with the constant radius of the nascent cluster. In the equation above, V_0 means the reference potential corresponding to the sum of potential self-energies (Coulomb plus surface) of each fragment in the asymptotic configuration.

B. Gamow factor and decay half-life

The quantum transition rate from the initial to final state of the system has been determined by reducing the problem to the one-dimensional barrier penetrability, similarly to Gamow alpha-decay theory [16]. This penetrability factor is calculated with the assumption that the system tunnels a barrier equal to $V-Q$. Shell effects on the nuclear masses manifested in the Q value [already used in Eq. (8)] are here reflected in the height and width of the effective barrier. The penetrability factor is calculated by

$$\mathcal{P}=\exp\left[-\frac{2}{\hbar}\int_{\zeta_0}^{\zeta_C}\sqrt{2\mu[V(\zeta)-Q]}d\zeta\right]\ . \tag{14}$$

The action integral in the penetrability factor is evaluated by using the variable of the model, ζ. The limits of the integral are the inner turning point

$$\zeta_0=R_p-\bar{R}_1\ , \tag{15}$$

and the outer one

$$\zeta_c=Z_1Z_2e^2/Q\ . \tag{16}$$

Finally, the decay rate is calculated as

$$\lambda=\lambda_0\mathcal{P}\ . \tag{17}$$

The characteristic time scale of surface oscillations in the initial state of the system is used to define the preexponential factor λ_0 in Eq. (17). The values of Shi and Swiatecki [21] with an odd-A parent nuclei hindrance effect,

$$\lambda_0=\begin{cases}10^{20}\ \mathrm{s}^{-1}, & A=\text{odd}\ ,\\ 10^{22}\ \mathrm{s}^{-1}, & A=\text{even}\ ,\end{cases} \tag{18}$$

have been used in the present work. With this preexponential factor fixed, the half-life is promptly calculated by

$$\tau=\ln 2/\lambda\ . \tag{19}$$

C. Radii and effective mass

The final radii of the fragments should be given by

$$\bar{R}_i=\left[\frac{Z_i}{Z_p}\right]^{1/3}R_p\ , \tag{20}$$

to be consistent with the uniform charge distribution considered in the Coulomb potential. The radius of the parent nucleus is determined by the simple formula

$$R_p = r_0 A_p^{1/3} , \tag{21}$$

setting $r_0 = 1.37$ fm in all calculations.

With the Werner-Wheeler approximation for the velocity field of nuclear fluid in the prescission phase, we can obtain an expression for the kinetic energy of the system [11,22]. The constraint expressed by Eqs. (1) and (2), and the condition of constant radius for the cluster, reduce the kinetic-energy expression to a quadratic form only in the velocity $\dot{\zeta}$. From this expression we get the effective mass for the degree of freedom ζ. In the center-of-mass frame we have, for this effective mass,

$$m_{\text{eff}} = \sum_{i=1,2} \rho_i \left\{ \frac{(z_i')^2 v_i}{\pi} + 2\times(-1)^i z_i' R_i R_i' (R_i + d_i)^2 + \frac{(R_i R_i')^2}{2} \left[\frac{4R_i^2}{h_i} - 9R_i - 7d_i + 12R_i \ln\left[\frac{2R_i}{h_i} \right] \right] \right\} , \tag{22}$$

where the mass density of each spherical segment is

$$\rho_i = 3M_i/(4\pi \bar{R}_i^3) , \tag{23}$$

and

$$z_1' = -\tfrac{1}{2}[3v_2 + \pi a^2 (R_1 + d_1)]/(v_1 + v_2), \quad z_2' = z_1' + 1 ,$$

$$R_1' = 0, \quad R_2' = -\frac{1}{2}\frac{h_2}{R_2} ,$$

$$d_1 = \zeta - \xi, \quad d_2 = \xi ,$$

$$h_1 = R_1 - \zeta + \xi, \quad h_2 = R_2 - \xi .$$

The primes in the above expressions mean the derivative with respect to the variable ζ, and

$$v_i = \frac{\pi}{3}(R_i + d_1)^2 (R_i + h_i)$$

is the volume of each spherical segment. We have used this effective mass as the reduced mass μ in Eq. (14), defining the penetrability factor. Although the expression for the effective mass changes for different choices of coordinates and frame, it should be noted that the result for the decay rate remains independent of these arbitrary choices [22]. In Fig. 3 we show the values of the effective mass as calculated by (22) for different cluster emission modes. Towards the asymptotic configuration of separated spheres, the effective mass reaches the reduced mass of the final fragments, $\bar{\mu}$.

III. RESULTS AND DISCUSSIONS

The calculated half-life for all cluster emission processes observed up to now are shown in Fig. 4. The thick line in the figure corresponds to our calculated result, and the open circles are the experimental data taken from recent review articles [23,24]. The present results are for a zero orbital angular momentum of the fragments. The decay modes and the values for the half-lives are presented in Table I, where the reactions with the same cluster emis-

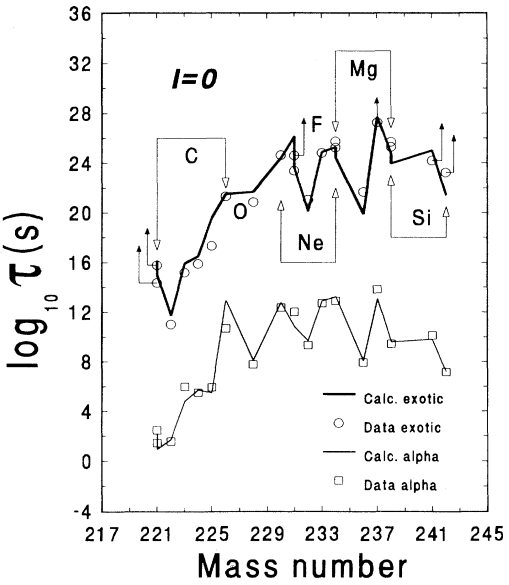

FIG. 4. Half-life for the exotic and α decays. In the upper region of the graph the thick line connects the calculated values of half-life for the exotic decays listed in Table I. The experimental data are shown by circles, and the arrows attached to six points indicate that these are only lower limits determined experimentally. The error bar for the other data is comparable to circle size. The thin line in the lower region connects the calculated values of half-life for α-decay mode of the exotic decay parent nuclei. The data for α-decay half-lives are shown by squares, with error bar smaller than the square size.

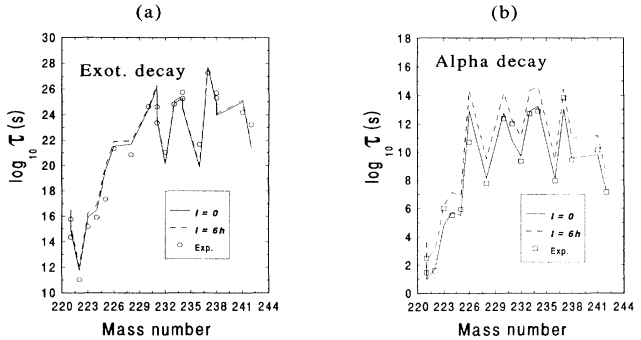

FIG. 5. Half-life calculated with the inclusion of the centrifugal barrier. The solid line in (a) presents the half-life of exotic decays for $l = 0$, and the dashed line is for $l = 6\hbar$. (b) is the same, but for α decay.

TABLE I. Decay reactions and half-lives. The second column lists the logarithm of the exotic decay half-life, taken from Refs. [23,24]. The third column lists the logarithm of the α-decay half-life of the parent nuclei listed in the first column (data were taken from Ref. [25]). The respective present calculated results are given in the last two columns.

	Experimental results		Theoretical results	
Decay reaction	$\log_{10}\tau^{exot}(s)$	$\log_{10}\tau^{\alpha}(s)$	$\log_{10}\tau^{exot}(s)$	$\log_{10}\tau^{\alpha}(s)$
$^{221}Fr\rightarrow{}^{14}C+{}^{207}Tl$	>15.77[a]	2.5±0.2	16.21	2.21
$^{221}Ra\rightarrow{}^{14}C+{}^{207}Pb$	>14.35[a]	1.45±0.03	14.98	0.95
$^{222}Ra\rightarrow{}^{14}C+{}^{208}Pb$	11.02±0.06	1.58±0.05	11.72	1.73
$^{223}Ra\rightarrow{}^{14}C+{}^{209}Pb$	15.20±0.05	5.995±0.001	15.92	4.80
$^{224}Ra\rightarrow{}^{14}C+{}^{210}Pb$	15.90±0.12	5.50±0.04	16.50	5.73
$^{225}Ac\rightarrow{}^{14}C+{}^{211}Bi$	17.34±0.30	5.94±0.04	19.59	5.48
$^{226}Ra\rightarrow{}^{14}C+{}^{212}Pb$	21.33±0.20	10.703±0.002	21.51	12.90
$^{228}Th\rightarrow{}^{20}O+{}^{208}Pb$	20.86±0.30	7.781±0.001	21.69	8.11
$^{231}Pa\rightarrow{}^{23}F+{}^{208}Pb$	>24.61[a]	12.014±0.001	26.14	10.80
$^{230}Th\rightarrow{}^{24}Ne+{}^{206}Hg$	24.64±0.07	12.376±0.001	24.39	12.77
$^{231}Pa\rightarrow{}^{24}Ne+{}^{207}Tl$	23.38±0.08	12.014±0.001	23.60	10.80
$^{232}U\rightarrow{}^{24}Ne+{}^{208}Pb$	21.06±0.10	9.337±0.001	20.10	9.70
$^{233}U\rightarrow{}^{25}Ne+{}^{208}Pb$	24.82±0.15	12.701±0.005	24.88	12.89
$^{234}U\rightarrow{}^{24}Ne+{}^{210}Pb$	25.25±0.05	12.889±0.001	25.26	13.22
$^{234}U\rightarrow{}^{28}Mg+{}^{206}Hg$	25.75±0.06	12.889±0.001	24.43	13.22
$^{236}Pu\rightarrow{}^{28}Mg+{}^{208}Pb$	21.68±0.15	7.954±0.001	19.90	8.10
$^{237}Np\rightarrow{}^{30}Mg+{}^{207}Tl$	>27.27[a]	13.829±0.002	27.68	13.05
$^{238}Pu\rightarrow{}^{28}Mg+{}^{210}Pb$	25.70±0.25	9.4423±0.0004	23.96	9.59
$^{238}Pu\rightarrow{}^{32}Si+{}^{206}Hg$	25.30±0.16	9.4423±0.0004	23.96	9.59
$^{241}Am\rightarrow{}^{34}Si+{}^{207}Tl$	>24.20[a]	10.135±0.0005	25.01	9.79
$^{242}Cm\rightarrow{}^{34}Si+{}^{208}Pb$	>23.24	7.1485±0.0002	24.01	7.35

[a]Taken from Ref. [23].

sion are grouped in blocks. In Fig. 4, the data of a given group are embraced by two connected open arrows.

Without any modification in the model (changing solely the input data for masses), all the calculations have been performed for α particle emission from each parent nucleus listed in Table I. The results for this essay are presented as the thin line in Fig. 4. The corresponding numerical values and experimental data are also presented in Table I. The experimental data for α decay have been taken from a table of radioactive isotopes [25], and are represented by open squares in Fig. 4. For α decay it should be remembered that angular momentum is not completely negligible for various decays, and it might correct some small deviations from our results for $l=0$ to the experimental data.

In Fig. 5 we show how sensitive the present results are to the effect of the centrifugal potential, if one includes V_l after the scission point. We can see in Fig. 5(a) that the effect is negligible for exotic decays, as was pointed out before. For α decay it appears significant, as evidenced by Fig. 5(b).

IV. CONCLUSIONS AND FINAL REMARKS

We have analyzed the half-life for the exotic decay in the framework of an effective fissionlike description for the process. The Coulomb energy was calculated analytically for the molecular phase of the system, from a double-intersecting-spheres parametrization for the deformed nuclear system.

The Werner-Wheeler approximation for the velocity field of nuclear fluid in the prescission phase defines the mass coefficient in the Gamow factor of the one-dimensional barrier penetrability calculation. The effective character of the model is marked by the surface tension defined in Eq. (8). At this point we have noted that nuclear radii are involved in this definition, so the nuclear radius parameter r_0 also controls the intensity of the surface potential. Since we are not using effects of proximity force [19,21] to the potential explicitly, we have to compensate for such effects by an appropriate intensity of our surface term. This fact justifies our choice of $r_0=1.37$ fm. Finally, it is remarked that we have fixed this r_0 value in all calculations for both exotic and α-decay disintegration modes studied in the present work.

ACKNOWLEDGMENTS

The authors are grateful for fruitful discussions with O. A. P. Tavares, C. E. Aguiar, and E. L. Medeiros during the development of the present work. One of us (M.G.) would like to thank the partial support of the Brazilian CNPq.

[1] H. G. de Carvalho, J. B. Martins, I. O. de Souza, and O. A. P. Tavares, Ann. Acad. Bras. Cienc. **47**, 567 (1975); **48**, 205 (1976).
[2] I. O. de Souza, M.Sc. thesis, Centro Brasileiro de Pesquisas Físicas, 1975 (unpublished).
[3] O. A. P. Tavares, doctoral thesis, Centro Brasileiro de Pesquisas Físicas, 1978 (unpublished).
[4] A. Săndulescu and W. Greiner, J. Phys. G **3**, L189 (1977).
[5] A. Săndulescu, H. J. Lustig, J. Hahn, and W. Greiner, J. Phys. G **4**, L279 (1978).
[6] A. Săndulescu, D. N. Poenaru, and W. Greiner, Fiz. Elem. Chastits At. Yadra **11**, 1334 (1980) [Sov. J. Part. Nucl. **11**, 528 (1980)].
[7] H. J. Rose and G. A. Jones, Nature (London) **307**, 245 (1984).
[8] D. V. Aleksandrov, A. F. Belyatskii, Yu. A. Glukhov, E. Yu. Nikol'skii, B. G. Novatskii, A. A. Ogloblin, and D. N. Stepanov, Pis'ma Zh. Eksp. Teor. Fiz. **40**, 152 (1984) [JETP Lett. **40**, 909 (1984)].
[9] D. N. Poenaru, M. Ivascu, and D. Mazilu, Comput. Phys. Commun. **19**, 205 (1980).
[10] D. N. Poenaru and M. Ivascu, J. Phys. (Paris) **45**, 1099 (1984).
[11] G. A. Pic-Pichac, Yad. Fiz. **44**, 1421 (1986) [Sov. J. Nucl. Phys. **44**, 923 (1986)].
[12] E. Hourani, M. Hussonnois, and D. N. Poenaru, Ann. Phys. Fr. **14**, 311 (1989).
[13] D. N. Poenaru, W. Greiner, M. Ivascu, D. Mazilu, and I. H. Plonski, Z. Phys. A **325**, 435 (1986).
[14] G. Shanmugam and B. Kamalaharan, Phys. Rev. C **41**, 1742 (1990).
[15] M. Gaudin, J. Phys. **35**, 885 (1974).
[16] G. Gamow, Z. Phys. **51**, 204 (1928).
[17] B. Buck, A. C. Merchant, and S. M. Perez, Nucl. Phys. **A512**, 483 (1990).
[18] A. H. Wapstra and G. Audi, Nucl. Phys. **A432**, 1 (1985).
[19] Yi-Jin Shi and W. J. Swiatecki, Phys. Rev. Lett. **54**, 300 (1985).
[20] H. G. de Carvalho, J. B. Martins, and O. A. P. Tavares, Phys. Rev. C **34**, 2261 (1986).
[21] Yi-Jin Shi and W. J. Swiatecki, Nucl. Phys. **A464**, 205 (1987).
[22] D. N. Poenaru, J. A. Maruhn, W. Greiner, M. Ivascu, D. Mazilu, and I. Ivascu, Z. Phys. A **333**, 291 (1989).
[23] P. B. Price, Nucl. Phys. **A502**, 41C (1989), and references therein.
[24] A. Săndulescu and W. Greiner, Rep. Prog. Phys. **55**, 1423 (1992), and references therein.
[25] E. Browne and R. B. Firestone, *Table of Radioactive Isotopes* (Wiley, New York, 1986).